



HAL
open science

A split-and-merge approach for hyperspectral band selection

Shaheera Rashwan, Nicolas Dobigeon

► **To cite this version:**

Shaheera Rashwan, Nicolas Dobigeon. A split-and-merge approach for hyperspectral band selection. *IEEE Geoscience and Remote Sensing Letters*, 2017, 14 (8), pp.1378-1382. 10.1109/LGRS.2017.2713462 . hal-01887849

HAL Id: hal-01887849

<https://hal.science/hal-01887849>

Submitted on 4 Oct 2018

HAL is a multi-disciplinary open access archive for the deposit and dissemination of scientific research documents, whether they are published or not. The documents may come from teaching and research institutions in France or abroad, or from public or private research centers.

L'archive ouverte pluridisciplinaire **HAL**, est destinée au dépôt et à la diffusion de documents scientifiques de niveau recherche, publiés ou non, émanant des établissements d'enseignement et de recherche français ou étrangers, des laboratoires publics ou privés.



Open Archive Toulouse Archive Ouverte

OATAO is an open access repository that collects the work of Toulouse researchers and makes it freely available over the web where possible

This is an author's version published in:
<http://oatao.univ-toulouse.fr/n° de post 19069>

Official URL: <https://ieeexplore.ieee.org/document/7967677/>
<http://dx.doi.org/10.1109/LGRS.2017.2713462>

To cite this version:

Rashwan, Shaheera and Dobigeon, Nicolas *A split-and-merge approach for hyperspectral band selection*. (2017) IEEE Geoscience and Remote Sensing Letters, 14 (8). 1378-1382. ISSN 1545-598X

Any correspondence concerning this service should be sent to the repository administrator: tech-oatao@listes-diff.inp-toulouse.fr

A Split-and-Merge Approach for Hyperspectral Band Selection

Shaheera Rashwan and Nicolas Dobigeon, *Senior Member, IEEE*

Abstract—The problem of band selection (BS) is of great importance to handle the curse of dimensionality for hyperspectral image (HSI) applications (e.g., classification). This letter proposes an unsupervised BS approach based on a split-and-merge concept. This new approach provides relevant spectral sub-bands by splitting the adjacent bands without violating the physical meaning of the spectral data. Next, it merges highly correlated bands and sub-bands to reduce the dimensionality of the HSI. Experiments on three public data sets and comparison with state-of-the-art approaches show the efficiency of the proposed approach.

Index Terms—Band selection (BS), data reduction, hyperspectral image (HSI).

I. INTRODUCTION

HYPERSPECTRAL images (HSIs) contain hundreds of continuous spectral bands, which are beneficial to remote sensing applications, such as image classification and target detection [1], [2]. However, a large number of spectral bands can result in a prohibitive computational complexity of HSI analysis algorithms. More importantly, this high number of bands leads to the so-called *curse of dimensionality*, also known as Hughes phenomenon [3], which, e.g., dramatically impacts the performance of the supervised classifiers [4]. Thus, band selection (BS) is an issue of high importance for HSI classification, which can be addressed by removing the highly correlated bands or the bands identified as those containing less significant information. Depending on the amount of available *a priori* knowledge regarding the HSI to be processed, the existing BS methods can fall into two distinct categories: supervised [5]–[7] and unsupervised approaches [8]–[15]. The labeled samples enable the supervised methods to take the spectral similarity between different classes into account. They can generally achieve better classification performance than unsupervised methods. For example, a BS method based on mutual information (MI) has been proposed in [5]. More recently, Yin *et al.* [6] suggested a new separability criterion, namely, the spectral separability index, to identify the relevant bands. Yang *et al.* [7] proposed a supervised BS algorithm that makes use of the known class

signatures without examining the original bands nor needing class training samples.

However, implementing supervised BS requires the availability of reliable labeled samples, which may be a difficult and tedious task. Therefore, unsupervised BS methods have been demonstrated to be more appropriate in applicative scenarios since they do not require any prior information about the different classes. Mojaradi *et al.* [8] derived an innovative BS method, called prototype space BS, based only on some class spectra. Also, Martínez-Usó *et al.* [9] proposed a technique that is based on a hierarchical clustering structure to group bands to minimize the intracluster variance while maximizing the intercluster variance. Adopting a spectral unmixing perspective [16], Du and Yang [10] proposed the application of those similarity-based endmember extraction algorithms for BS. Feng *et al.* [11] proposed a formal probabilistic memetic algorithm for BS, which is able to adaptively control the degree of global exploration against local exploitation throughout the search procedure. Nakamura *et al.* [12] addressed the problem of BS in hyperspectral remote sensing images by resorting to nature-inspired algorithms. Chang *et al.* [13] presented a parallel BS approach, referred to as parallel simulated annealing BS, for high-dimensional remote sensing images. Cariou *et al.* [14] proposed an unsupervised approach to band reduction for HSIs named BandClust, which stands for band clustering. It consists in splitting the initial range of spectral bands into disjoint clusters or sub-bands. Sui *et al.* [15] proposed a new method that integrates both the overall accuracy (OA) and redundancy into the BS process by formulating an optimization model. Recently, Wang *et al.* [17] proposed a novel salient BS method that is based on manifold ranking to ensure an appropriate measurement of band difference. Finally, Yuan *et al.* [18] proposed a new framework named dual-clustering-based BS by context analysis that considers the context information of bands in the process of dual clustering.

All previous works dedicated to HSI BS are based on selection procedures of the original bands. Such techniques may produce unreliable results in particular when the spectral ranges associated with these bands are not sufficiently narrow. Conversely, this letter proposes an unsupervised approach for HSI BS, which is based on band clustering by split-and-merge steps. The main novelty of this letter consists in splitting the original range of spectral bands into sub-bands and then merging the resulting highly correlated bands.

This letter is organized as follows. The proposed method is detailed in Section II. In Section III, some experimental results obtained on three public hyperspectral data sets are

This work was supported by EU FP7 through the ERANETMED JC-WATER Program under MapInvPlnt Project ANR-15-NMED-0002-02. (Corresponding author: Nicolas Dobigeon.)

S. Rashwan is with the Informatics Research Institute, Alexandria, Egypt (e-mail: srashwan@mucsat.sci.eg).

N. Dobigeon is with IRIT/INP-ENSEEIH, University of Toulouse, 31000 Toulouse, France (e-mail: nicolas.dobigeon@enseeiht.fr).

Color versions of one or more of the figures in this letter are available online at <http://ieeexplore.ieee.org>.

reported. Section IV concludes this letter and provides some future works.

II. PROPOSED SPLIT-AND-MERGE BAND SELECTION METHOD

Let us consider $\mathbf{X} \triangleq [\mathbf{x}_1, \dots, \mathbf{x}_L]^T \in \mathbb{R}^{L \times P}$ the lexicographically indexed HSI composed of P pixels and L bands, where $\mathbf{x}_\ell \triangleq [x_{\ell,1}, \dots, x_{\ell,P}]^T$ is the image observed in the ℓ th band corresponding to a wavelength λ_ℓ . This section details the proposed split-and-merge algorithm for hyperspectral BS as a two-stage approach beginning, first, by splitting low-correlated bands and then merging high-correlated bands. These two steps are described in what follows.

A. Splitting Step

The iterative splitting process consists in sequentially examining HSI bands to identify pairs of weakly correlated adjacent bands ℓ and $\ell + 1$. These uncorrelated HSI bands are subsequently split to build a synthetic HSI $\check{\mathbf{X}} \triangleq [\check{\mathbf{x}}_1, \dots, \check{\mathbf{x}}_{\check{L}}]^T \in \mathbb{R}^{\check{L} \times P}$, where $\check{L} \geq L$ is the total number of (possibly real and virtual) spectral bands of the HSI recovered by the process. More precisely, let $\check{\mathbf{X}}^{(t)}$ denote the current state of the synthetic HSI after the t th iteration of the splitting process. The single-band images $\check{\mathbf{x}}_\ell^{(t)}$ and $\check{\mathbf{x}}_{\ell+1}^{(t)}$ in bands ℓ and $\ell + 1$ corresponding to the wavelengths $\lambda_\ell^{(t)}$ and $\lambda_{\ell+1}^{(t)}$, respectively, are split if the sample-based Pearson correlation coefficient $\check{r}_{\ell,\ell+1}^{(t)}$ between $\check{\mathbf{x}}_\ell^{(t)}$ and $\check{\mathbf{x}}_{\ell+1}^{(t)}$ is lower than a given threshold value ρ

$$\check{r}_{\ell,\ell+1}^{(t)} < \rho. \quad (1)$$

One recalls that $\check{r}_{\ell,\ell+1}^{(t)}$ is given by [19]

$$\check{r}_{\ell,\ell+1}^{(t)} = \frac{\sum_{p=1}^P (\check{x}_{\ell,p}^{(t)} - \bar{\check{x}}_\ell^{(t)})(\check{x}_{\ell+1,p}^{(t)} - \bar{\check{x}}_{\ell+1}^{(t)})}{\sqrt{\sum_{p=1}^P (\check{x}_{\ell,p}^{(t)} - \bar{\check{x}}_\ell^{(t)})^2} \sqrt{\sum_{p=1}^P (\check{x}_{\ell+1,p}^{(t)} - \bar{\check{x}}_{\ell+1}^{(t)})^2}} \quad (2)$$

where $\check{x}_{\ell,p}$ and $\bar{\check{x}}_\ell = (1/P) \sum_{p=1}^P \check{x}_{\ell,p}$ are the intensity of the p th pixel and the mean pixel intensity, respectively, in the ℓ th band. These two decorrelated images $\check{\mathbf{x}}_\ell^{(t)}$ and $\check{\mathbf{x}}_{\ell+1}^{(t)}$ are then split to produce two additional virtual images $\check{\mathbf{x}}_{\ell+1}^{(t+1)}$ and $\check{\mathbf{x}}_{\ell+2}^{(t+1)}$ of the $(t + 1)$ th-iterated HSI image $\check{\mathbf{X}}^{(t+1)}$ as follows:

$$\begin{cases} \check{\mathbf{x}}_\ell^{(t+1)} = \check{\mathbf{x}}_\ell^{(t)} \\ \check{\mathbf{x}}_{\ell+1}^{(t+1)} = \alpha(\check{\mathbf{x}}_\ell^{(t)} + \check{\mathbf{x}}_{\ell+1}^{(t)}) \\ \check{\mathbf{x}}_{\ell+2}^{(t+1)} = (1 - \alpha)(\check{\mathbf{x}}_\ell^{(t)} + \check{\mathbf{x}}_{\ell+1}^{(t)}) \\ \check{\mathbf{x}}_{\ell+3}^{(t+1)} = \check{\mathbf{x}}_{\ell+1}^{(t)} \end{cases} \quad (3)$$

where $\alpha \in (0, 1)$ is a given weighting parameter. It is worthy to note that the set of virtual composite images $\{\check{\mathbf{x}}_{\ell+1}^{(t+1)}, \check{\mathbf{x}}_{\ell+2}^{(t+1)}\}$ is expected to hold the same amount of information as the pair of split images $\{\check{\mathbf{x}}_\ell^{(t)}, \check{\mathbf{x}}_{\ell+1}^{(t)}\}$. The band indexes $(\ell + 1)$ and $(\ell + 2)$ of the composite images correspond to wavelengths $\lambda_{\ell+1}^{(t+1)}$ and $\lambda_{\ell+2}^{(t+1)}$ chosen in the range $(\lambda_\ell^{(t)}, \lambda_{\ell+1}^{(t)})$ as

$$\begin{cases} \lambda_{\ell+1}^{(t+1)} = \lambda_\ell^{(t)} + \delta\lambda^{(t)} \\ \lambda_{\ell+2}^{(t+1)} = \lambda_{\ell+1}^{(t)} - \delta\lambda^{(t)} \end{cases} \quad (4)$$

where the wavelength stepsize $\delta\lambda^{(t)}$ is adjusted along the algorithm iterations following a geometrical updating rule, $\delta\lambda^{(t+1)} = \alpha\delta\lambda^{(t)}$. Finally, if the pair of images $\{\mathbf{x}_\ell^{(t)}, \mathbf{x}_{\ell+1}^{(t)}\}$ has not been split, i.e., $r_{\ell,\ell+1}^{(t)} > \rho$, then only the image $\mathbf{x}_\ell^{(t)}$ is included into the new state of the synthetic HSI, i.e., $\check{\mathbf{x}}_\ell^{(t+1)} = \check{\mathbf{x}}_\ell^{(t)}$. The splitting procedure ends at iteration T_{\max} when the wavelength stepsize $\delta\lambda^{(T_{\max})}$ falls below a minimum value, namely, $\delta\lambda_{\min}$. The whole procedure is sketched in Algorithm 1.

Algorithm 1 Splitting Process

Input: Observed image \mathbf{X} .

Threshold parameter ρ .

Weighting parameter α .

Minimum stepsize $\delta\lambda_{\min}$ and $\delta\lambda_{\text{init}}$ initial values.

Initializations:

1: $t \leftarrow 1$

2: $\delta\lambda^{(t)} \leftarrow \delta\lambda_{\text{init}}$

3: $\check{\mathbf{X}}^{(t)} \leftarrow \mathbf{X}$

4: $\check{L} \leftarrow L$

Iterations:

5: **while** $\delta\lambda^{(t)} > \delta\lambda_{\min}$ **do**

6: $\ell \leftarrow 1$

7: **while** $\ell < \check{L}$ **do**

8: Compute $r_{\ell,\ell+1}^{(t)}$ following (2)

9: **if** $r_{\ell,\ell+1}^{(t)} < \rho$ **then**

10: $\check{\mathbf{x}}_\ell^{(t+1)} \leftarrow \check{\mathbf{x}}_\ell^{(t)}$

11: $\check{\mathbf{x}}_{\ell+1}^{(t+1)} \leftarrow \alpha(\check{\mathbf{x}}_\ell^{(t)} + \check{\mathbf{x}}_{\ell+1}^{(t)})$

12: $\check{\mathbf{x}}_{\ell+2}^{(t+1)} \leftarrow (1 - \alpha)(\check{\mathbf{x}}_\ell^{(t)} + \check{\mathbf{x}}_{\ell+1}^{(t)})$

13: $\check{\mathbf{x}}_{\ell+3}^{(t+1)} \leftarrow \check{\mathbf{x}}_{\ell+1}^{(t)}$

14: $\check{L} \leftarrow \check{L} + 2$

15: $\ell \leftarrow \ell + 3$

16: **else**

17: $\check{\mathbf{x}}_\ell^{(t+1)} \leftarrow \check{\mathbf{x}}_\ell^{(t)}$

18: $\ell \leftarrow \ell + 1$

19: **end if**

20: **end while**

21: $\delta\lambda^{(t+1)} \leftarrow \alpha\delta\lambda^{(t)}$

22: $t \leftarrow t + 1$

23: **end while**

Output: The HSI $\check{\mathbf{X}} = \check{\mathbf{X}}^{(t-1)}$ after the splitting process.

B. Merging Step

Once a synthetic HSI image $\check{\mathbf{X}}$ with an extended number \check{L} of bands has been obtained from the splitting process (see Section II-A), these \check{L} spectral bands follow a merging process that aims at gathering most of the information into a significantly lower number of bands \hat{L} , with $\hat{L} \leq L \leq \check{L}$. This merging process consists in successively analyzing the spectral bands of $\check{\mathbf{X}}$ to identify the most correlated ones, following the opposite decision rule specified in (1). This set of correlated images is then fused to produce a single-band image according to a hyperspectral

fusion process. Hyperspectral fusion has motivated plenty of research contributions [20]–[23]. In this letter, the fusion process is conducted by averaging the multiple single-band images to be merged

$$\hat{\mathbf{x}}_\ell = \frac{1}{|\mathcal{I}_\ell|} \sum_{k=1}^{|\mathcal{I}_\ell|} \check{\mathbf{x}}_k \quad (5)$$

where $\hat{\mathbf{x}}_\ell$ denotes the ℓ th band after the merging process, \mathcal{I}_ℓ is the set of indices corresponding to the bands $\check{\mathbf{x}}_k$ to be merged, and $|\cdot|$ denotes the cardinality. The whole merging process is provided in Algorithm 2. Note that the fusing step is only denoted by $\text{fuse}\{\cdot\}$ since any other competing fusion algorithm can be used in place of the considered empirical average.

Algorithm 2 Merging Process

Input: HSI image $\check{\mathbf{X}}$ after splitting process.
Threshold parameter ρ .

Initializations:

- 1: $t \leftarrow 1$
- 2: $\ell \leftarrow 1$
- 3: $\hat{\mathcal{L}} \leftarrow \check{\mathcal{L}}$

Iterations:

- 4: **while** $\ell < \hat{\mathcal{L}}$ **do**
- 5: $\ell \leftarrow 1$
- 6: $\mathcal{I}_\ell \leftarrow \{\ell\}$
- 7: **for** $k \in \{\ell + 1, \dots, \check{\mathcal{L}}\}$ **do**
- 8: Compute $\check{r}_{\ell,k}$ following (2)
- 9: **if** $r_{\ell,k} > \rho$ **then**
- 10: $\mathcal{I}_\ell \leftarrow \mathcal{I}_\ell \cup \{k\}$
- 11: $\hat{\mathcal{L}} \leftarrow \hat{\mathcal{L}} - 1$
- 12: **end if**
- 13: **end for**
- 14: $\hat{\mathbf{x}}_\ell \leftarrow \text{fuse}\{\check{\mathbf{x}}_k; k \in \mathcal{I}_\ell\}$
- 15: $\ell \leftarrow \ell + 1$
- 16: **end while**

Output: The HSI $\hat{\mathbf{X}} \triangleq [\hat{\mathbf{x}}_1, \dots, \hat{\mathbf{x}}_{\hat{\mathcal{L}}}]^T$ after the merging process.

III. EXPERIMENTAL RESULTS

This section reports some experiments conducted using three HSIs described in Section III-A. The proposed split-and-merge BS algorithm has been compared with other fusion approaches: minimum noise fraction (MNF) [24], feature selection based on feature similarity (FSFS) [25], Ward’s linkage strategy using MI (WaLuMI), and Ward’s linkage strategy using divergence (WaLuDi) [9]. For the WaLuMi and WaLuDi methods, the number of bands needs to be *a priori* fixed. To establish a fair comparison, in the conducted experiments, it is selected as the same value as the one recovered by the proposed split-and-merge algorithm. For each data set, the selected bands are subsequently fused using the particle swarm optimization image fusion proposed in [26] with the root-mean-square error as the objective function to be minimized. The performance of each BS approach is assessed by



Fig. 1. (Left) Composite color image of the Indian Pines AVIRIS image. (Right) Ground-truth class labels.

conducted supervised classification. More precisely, benefiting from the availability of ground truth associated with the considered HSI, support vector machine (SVM) classifiers are implemented, exploiting the fused band resulting from the BS procedures. In this letter, the SVM-based classification task has been conducted thanks to the LIBSVM software [27] with a kernel chosen as the Gaussian radial basis function. Classification performance is monitored using the OA and Cohen’s kappa index. The number of bands recovered by each BS method is also provided as a complementary information, which allows the tradeoff between the number of selected bands and the amount of relevant information (assessed by classification performance) to be evaluated. Note that, since the proposed method automatically infers the number of relevant bands, to provide fair comparison, the compared methods have been tailored to reach a result obtained with the same number of retrieved bands, by adjusting the corresponding algorithmic parameters.

A. Data Sets

The first hyperspectral data set considered is the so-called Indian Pines image acquired by the Airborne Visible/Infrared Imaging Spectrometer (AVIRIS). This image originally consists of 220 spectral bands in the 0.4–2.5- μm VNIR range [28]. Each band is a 145×145 pixel image. The corrected Indian Pines used in the conducted experiment has been reduced to only 200 bands after removing bands covering the region of water absorption. Fig. 1(left) shows a color composition of the scene, with spectral bands 28, 19, and 10 used for the red–green–blue (RGB) channels, respectively. For the performance assessment by SVM classification, the training set has been randomly selected as a 60% of the labeled pixels and the whole set of data has been used for computing the OA and kappa index. In the implementation of the proposed split-and-merge BS algorithm for the AVIRIS data set, the tuning parameters have been empirically selected after several trials as $\delta\lambda_{\min} = 0.1$ and $\rho = 0.8$ in the proposed split-and-merge BS algorithm.

The second hyperspectral data used have been acquired by the Reflective Optics System Imaging Spectrometer (ROSIS) over Pavia, consisting of 103 spectral bands in the range 430–770 nm [28]. Each band is a 610×340 pixel image. A color composite image of the scene is depicted in Fig. 2(left) where spectral bands 28, 19, and 10 are used for the RGB channels, respectively. Within the SVM classification, the size of randomly selected training set has been set as a 10% of the labeled pixels and the whole data have been used as test pixels for computing the OA and kappa figures of merit. For this

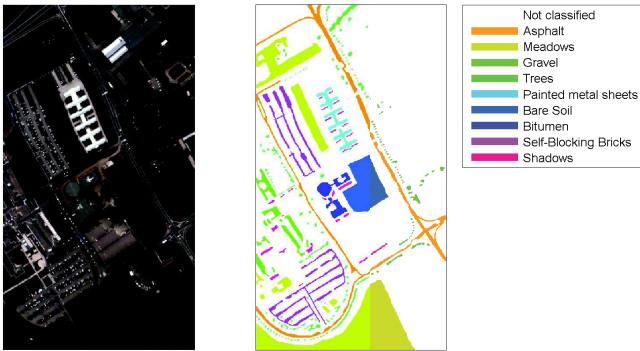


Fig. 2. (Left) Composite color image of the Pavia University ROSIS image. (Right) Ground-truth class labels.

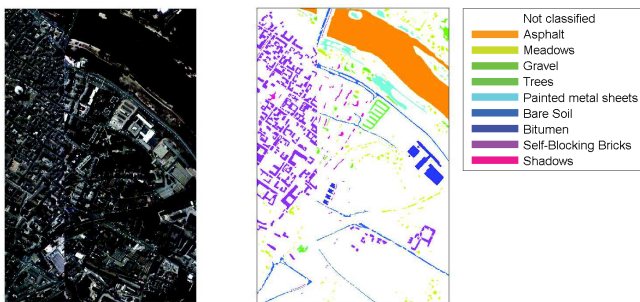


Fig. 3. (Left) Composite color image of the Pavia Center ROSIS image. (Right) Ground-truth class labels.

ROSIS data set, the minimum wavelength stepsize has been fixed as $\delta\lambda_{\min} = 0.5$ while the correlation threshold has been fixed as $\rho = 0.975$.

The third hyperspectral data used have been acquired over Pavia Center also by ROSIS with the same spectral characteristics reported above. Each band is a 1096×715 pixel image after removing spurious pixels. A color composite image of the scene is depicted in Fig. 3(left) where spectral bands 28, 19, and 10 are used for the RGB channels, respectively. Within the SVM classification, the size of randomly selected training set has been set as a 1% of the labeled pixels and the whole data have been used as test pixels for computing the OA and kappa figures of merit. Again, for this ROSIS data set, the minimum wavelength stepsize has been fixed as $\delta\lambda_{\min} = 0.5$ while the correlation threshold has been fixed as $\rho = 0.975$.

B. Results

This section reports and discusses the results obtained by the considered algorithms on the three data sets, namely, Indian Pines, Pavia University, and Pavia Center. Table I reports the OAs, kappa indices, and corresponding number of selected bands recovered by the other unsupervised BS methods (MNF, FSFS, WaluMi, and WaluDi) and the proposed split-and-merge approach (denoted S&M).

These results show that for the AVIRIS Indian Pines data set, the proposed split-and-merge algorithm provides better results in terms of OA and kappa index in comparison with the other four unsupervised BS methods (MNF, FSFS, WaluMi, and WaluDi) where the number of bands has been significantly

TABLE I
OA, KAPPA, AND NUMBER OF BANDS (#) FOR EACH METHOD
ON INDIAN PINES AND PAVIA DATA SETS

	Indian Pines		Pavia University		Pavia Center	
	OA (%)	Kappa	OA (%)	Kappa	OA (%)	Kappa
All bands	66.9250	0.4674	78.6268	0.0328	82.5563	0.2902
MNF	64.0951	0.4087	78.2650	0.0385	81.3110	0.2633
FSFS	64.0488	0.4047	78.7194	0.0325	80.8690	0.1717
WaluMi	64.1510	0.4126	78.6572	0.0368	81.2114	0.1940
WaluDi	42.0927	0.0662	78.6581	0.0356	81.8395	0.2460
S&M	64.9703	0.4189	78.7363	0.0352	81.9869	0.2664

reduced from 200 to 40 bands. For the ROSIS Pavia University data set, the split-and-merge algorithm performs better than the four unsupervised BS methods and also gives better results than the whole band set in terms of kappa indices. The new S&M performs better in terms of OA for the ROSIS data set when reducing the number of bands significantly from 103 to 28. Also, for the ROSIS Pavia Center data set, our new algorithm outperforms the four unsupervised BS methods and succeeds in reducing the number of selected bands from 103 to 29. Note that we adjusted the number of bands to be the same in our experiments to establish a fair comparison between our new algorithm and the four unsupervised BS methods.

IV. CONCLUSION

Although hyperspectral imaging provides a huge amount of information regarding the sensed scene, hyperspectral data-cubes are composed of highly correlated single-band images. This implies the need for designing efficient BS techniques to select the most informative bands and hence to reduce the computational efforts while decreasing the storage space. In this letter, we proposed a new unsupervised BS approach based on a split-and-merge concept. The new algorithm performed a split step once two adjacent spectral bands were detected as weakly correlated. The splitting step was conducted by creating two virtual sub-bands between the two original bands. This splitting procedure was repeated for the sub-bands as long as they are weakly correlated. In a second stage of the proposed algorithm, the algorithm applied a merge step by fusing all bands that are determined as highly correlated. The experiments conducted on three different public data sets, namely, AVIRIS Indian Pines, ROSIS Pavia University, and ROSIS Pavia Center images, showed the potential of the proposed split-and-merge approach. Future work includes investigations on the use of alternative correlation measures to be exploited within the split and merge steps. Furthermore, efforts will be dedicated to tune efficiently and in an unsupervised way the algorithmic parameters of the proposed split-and-merge technique (i.e., $\delta\lambda_{\min}$ and ρ). Since these parameters are expected to be highly dependent on the hyperspectral sensor, a strategy would be to learn beforehand optimal parameter values associated with different HSIs. Note that the values reported in Section III for the AVIRIS and ROSIS data sets can be useful to analyze other data sets coming from these two particular sensors.

REFERENCES

- [1] C.-I. Chang, *Hyperspectral Imaging: Techniques for Spectral Detection and Classification*. New York, NY, USA: Kluwer, 2003.
- [2] C.-I. Chang, *Hyperspectral Data Exploitation: Theory and Applications*. Hoboken, NJ, USA: Wiley, 2007.
- [3] G. Hughes, "On the mean accuracy of statistical pattern recognizers," *IEEE Trans. Inf. Theory*, vol. 14, no. 1, pp. 55–63, Jan. 1968.
- [4] L. O. Jimenez and D. A. Landgrebe, "Supervised classification in high-dimensional space: Geometrical, statistical, and asymptotical properties of multivariate data," *IEEE Trans. Syst., Man, Cybern., C (Appl. Rev.)*, vol. 28, no. 1, pp. 39–54, Feb. 1998.
- [5] B. Guo, S. R. Gunn, R. I. Damper, and J. D. B. Nelson, "Band selection for hyperspectral image classification using mutual information," *IEEE Geosci. Remote Sens. Lett.*, vol. 3, no. 4, pp. 522–526, Oct. 2006.
- [6] J. Yin, Y. Wang, and Z. Zhao, "Optimal band selection for hyperspectral image classification based on inter-class separability," in *Proc. Symp. Photon. Optoelectron. (SOPO)*, Jun. 2010, pp. 1–4.
- [7] H. Yang, Q. Du, H. Su, and Y. Sheng, "An efficient method for supervised hyperspectral band selection," *IEEE Geosci. Remote Sens. Lett.*, vol. 8, no. 1, pp. 138–142, Jan. 2011.
- [8] B. Mojaradi, H. Emami, M. Varshosaz, and S. Jamali, "A novel band selection method for hyperspectral data analysis," *Int. Arch. Photogramm. Remote Sens. Spatial Inf. Sci.*, vol. 37, pp. 447–454, Jul. 2008.
- [9] A. Martínez-Usó, F. Pla, J. M. Sotoca, and P. García-Sevilla, "Clustering-based hyperspectral band selection using information measures," *IEEE Trans. Geosci. Remote Sens.*, vol. 45, no. 12, pp. 4158–4171, Dec. 2007.
- [10] Q. Du and H. Yang, "Similarity-based unsupervised band selection for hyperspectral image analysis," *IEEE Geosci. Remote Sens. Lett.*, vol. 5, no. 4, pp. 564–568, Oct. 2008.
- [11] L. Feng, A.-H. Tan, M.-H. Lim, and S. W. Jiang, "Band selection for hyperspectral images using probabilistic memetic algorithm," *Soft Comput.*, vol. 20, no. 12, pp. 4685–4693, Dec. 2016.
- [12] R. Y. M. Nakamura, L. M. G. Fonseca, J. A. Dos Santos, R. Da S Torres, X.-S. Yang, and J. P. Papa, "Nature-inspired framework for hyperspectral band selection," *IEEE Trans. Geosci. Remote Sens.*, vol. 52, no. 4, pp. 2126–2137, Apr. 2014.
- [13] Y.-L. Chang, K.-S. Chen, B. Huang, W.-Y. Chang, J. A. Benediktsson, and L. Chang, "A parallel simulated annealing approach to band selection for high-dimensional remote sensing images," *IEEE J. Sel. Topics Appl. Earth Observat. Remote Sens.*, vol. 4, no. 3, pp. 579–590, Mar. 2011.
- [14] C. Cariou, K. Chehdi, and S. L. Moan, "BandClust: An unsupervised band reduction method for hyperspectral remote sensing," *IEEE Geosci. Remote Sens. Lett.*, vol. 8, no. 3, pp. 565–569, May 2011.
- [15] C. Sui, Y. Tian, Y. Xu, and Y. Xie, "Unsupervised band selection by integrating the overall accuracy and redundancy," *IEEE Geosci. Remote Sens. Lett.*, vol. 12, no. 1, pp. 185–189, Jan. 2015.
- [16] J. M. Bioucas-Dias *et al.*, "Hyperspectral unmixing overview: Geometrical, statistical, and sparse regression-based approaches," *IEEE J. Sel. Topics Appl. Earth Observat. Remote Sens.*, vol. 5, no. 2, pp. 354–379, Apr. 2012.
- [17] Q. Wang, J. Lin, and Y. Yuan, "Salient band selection for hyperspectral image classification via manifold ranking," *IEEE Trans. Neural Netw. Learn. Syst.*, vol. 27, no. 6, pp. 1279–1289, Jun. 2016.
- [18] Y. Yuan, J. Lin, and Q. Wang, "Dual-clustering-based hyperspectral band selection by contextual analysis," *IEEE Trans. Geosci. Remote Sens.*, vol. 54, no. 3, pp. 1431–1445, Mar. 2016.
- [19] J. L. Rodgers and W. A. Nicewander, "Thirteen ways to look at the correlation coefficient," *Amer. Statist.*, vol. 42, no. 1, pp. 59–66, 1988.
- [20] R. B. Gomez, A. Jazaeri, and M. Kafatos, "Wavelet-based hyperspectral and multispectral image fusion," *Proc. SPIE*, vol. 4383, p. 36, Jun. 2001.
- [21] S. S. Bedi and R. Khandelwal, "Comprehensive and comparative study of image fusion techniques," *Int. J. Soft Comput. Eng.*, vol. 3, no. 1, pp. 2231–2307, Mar. 2013.
- [22] V. P. S. Naidu and J. R. Raol, "Pixel-level image fusion using wavelets and principal component analysis," *Defence Sci. J.*, vol. 58, no. 3, p. 338, May 2008.
- [23] S. Rashwan, H. A. Hassan, and N. Shawky, "An enhanced wavelet expectation-maximization algorithm for hyperspectral image segmentation," *Int. J. Imag. Robot.*, vol. 15, no. 3, pp. 150–163, 2015.
- [24] A. A. Green, M. Berman, P. Switzer, and M. D. Craig, "A transformation for ordering multispectral data in terms of image quality with implications for noise removal," *IEEE Trans. Geosci. Remote Sens.*, vol. 26, no. 1, pp. 65–74, Jan. 1988.
- [25] P. Mitra, C. A. Murthy, and S. K. Pal, "Unsupervised feature selection using feature similarity," *IEEE Trans. Pattern Anal. Mach. Intell.*, vol. 24, no. 3, pp. 301–312, Mar. 2002.
- [26] S. Rashwan, W. Sheta, and N. Dobigeon, "Spectral weighted image fusion using nature-inspired algorithms," submitted for publication.
- [27] C.-C. Chang and C.-J. Lin, "LIBSVM: A library for support vector machines," *ACM Trans. Intell. Syst. Technol.*, vol. 2, no. 3, p. 27, 2011.
- [28] Grupo de Inteligencia Computacional de la Universidad del País Vasco. (Feb. 2016). *Hyperspectral Remote Sensing Scenes*. [Online]. Available: <https://tinyurl.com/p8nv79f>